PARAMETRIC INVESTIGATION OF A HIGH-LIFT AIRFOIL AT HIGH REYNOLDS NUMBERS

John C. Lin*

NASA Langley Research Center, Hampton, VA 23681-0001

and

Chet J. Dominik†

McDonnell Douglas Aerospace, Long Beach, CA 90810-1870

Abstract

A new two-dimensional, three-element, advanced high-lift research airfoil has been tested in the NASA Langley Research Center's Low-Turbulence Pressure Tunnel at a chord Reynolds number up to 1.6×10^7. The components of this high-lift airfoil have been designed using a incompressible computational code (INS2D). The design was to provide high maximum-lift values while maintaining attached flow on the single-segment flap at landing conditions. The performance of the new NASA research airfoil is compared to a similar reference high-lift airfoil. On the new high-lift airfoil the effects of Reynolds number on slat and flap rigging have been studied experimentally, as well as the Mach number effects. The performance trend of the high-lift design is comparable to that predicted by INS2D over much of the angle-of-attack range. However, the code did not accurately predict the airfoil performance or the configuration-based trends near maximum lift where the compressibility effect could play a major role.

---

* Senior Research Engineer, Flow Modeling and Control Branch, Fluid Mechanics and Acoustics Division, Member AIAA.

† Engineer/Scientist Specialist, Subsonic Aerodynamics Technology Group, Advanced Transport Aircraft Development, Member AIAA.

Nomenclature

C_d = drag coefficient

C_l = lift coefficient

C_p = pressure coefficient

c = cruise or stowed airfoil chord

M = Mach number

Re_c = Reynolds number based on cruise chord c

x, y = coordinates along and normal to the chord direction, respectively

α = angle of attack

Subscripts

max = maximum value

min = minimum value

te = trailing-edge value

∞ = freestream value

Introduction

A major objective of aircraft manufacturers is to reduce aircraft cost. One possible way to reach that objective is to build simpler and cheaper high-lift systems (single-segment flaps). This presents a challenge to the high-lift aerodynamicist: to design a single-segment flap that maintains high levels of maximum lift while minimizing flow separation. Furthermore, by reducing the number of elements in the high-lift system and maintaining attached flow on the flap, aircraft noise will be reduced.

In the past several years there has been little two-dimensional data published about high Reynolds number component optimization.[1-4] There is a particular need to expand this database as well as the database for Reynolds number and Mach number effects on high-lift airfoils. New high-lift components were designed and fabricated to mate with the main-element spar of an

existing NASA supercritical research airfoil[5] to form the current high-lift research model. Using a state-of-the-art computational method,[6] a new slat, main-element's leading-edge, spoiler, flap shelf and single-segment flap were designed. These model parts were designed with the goal of maintaining high levels of maximum lift, while minimizing flow separation.

The primary objective of the current experiment was to expand the existing experimental database[1-4] of high-lift aerodynamic data for computational fluid dynamics code calibration. This paper describes the design of the new high-lift components and compares the current design code's predictions with the results of high Reynolds number wind-tunnel tests. The paper also explores the optimization of the component rigging (changes in gap and overhang) of the slat and flap as well as Reynolds number and Mach number effects on high-lift airfoils. All of the experimental results shown in this report were two-dimensional and obtained in the NASA Langley Research Center's Low-Turbulence Pressure Tunnel (LTPT).[7]

LTPT

The LTPT is a single-return, closed-loop wind tunnel that can be operated at pressures up to 10 atm, thus providing very high Reynolds number capability.[7] A diagram of the tunnel-circuit layout is shown in Fig. 1. The test section is 3 ft wide by 7.5 ft high by 7.5 ft long. Most of the testing was conducted at a freestream Mach number M_∞ of 0.20 and Reynolds numbers based on cruise (stowed) chord Re_c of 4.2, 9, and 16 x 10^6. The 4.2 x 10^6 Reynolds number case represents a typical wind-tunnel condition for full-span, three-dimensional tests. The 9 and 16 x 10^6 Reynolds number cases represent the flight conditions for an outboard and an inboard wing station, respectively, of a representative narrow-body transport.

To promote two-dimensional flow, a passive sidewall boundary-layer control (BLC) system was used.[8] The BLC system utilized the differential pressure between the test section and the atmosphere to provide suction (venting) of the sidewall boundary layer through porous endplates. Selection of the proper venting flow rate was based on an examination of spanwise pressure variations at several chordwise locations. For the configurations tested in the present investigation,

the trailing-edge flow was found to be substantially two dimensional, with a maximum spanwise variation in C_p (which was near the $C_{l,max}$) of 0.05 in the region between the flap brackets. The LTPT was designed with a large contraction ratio (17:1) and nine antiturbulence screens to produce extremely low-turbulence levels[9] (less than 0.5% for most cases). Because of the ability of the LTPT to provide flight Reynolds numbers for representative narrow-body transports, the model was tested transition-free (not fixed).

Model and Measurements

The NASA high-lift model is derived from an existing 12% thick supercritical airfoil of the energy efficient transport (EET) class[5] (shown in Fig. 2). This NASA EET cruise airfoil is similar, but 0.45%c thicker and has more (aft) camber than the cruise airfoil of Ref. 2 (Figs. 2 and 3). The NASA model spanned the width of the test section and had a clean (stowed) chord of 21.654 in. A diagram of the current three-element airfoil is shown in Fig. 4. The slat chord is 14.48%, the main-element chord is 83.06%, and the flap chord is 30% of the stowed airfoil chord. The current flap was very similar in shape to the flap of Ref. 4. It should be noted that Refs. 2 and 4 share the same cruise airfoil, but only Ref. 2 presented the cruise data. Hence, the high-lift data of Ref. 4 are being used throughout this paper for comparison with the current high-lift data; whereas the cruise data of Ref. 2 are being used herein for comparison with the current cruise data.

Surface pressures were made with over 156 pressure taps for the high-lift configuration. All pressure taps were connected to an electronically scanned pressure (ESP) measurement system for speedy data acquisition. Pressure orifices were located along the centerline of the model. Additional pressure taps were located in a spanwise row at chordwise stations of 5%c (on the slat), 74%c (on the main element), 87.4%c (on the flap), and the flap trailing edge to monitor two-dimensionality of the flow, as described earlier. Integration of the pressure measurements yielded the lift data presented herein. Using the Kline and McClintock method,[10] the uncertainty in $C_{l,max}$ was calculated to be approximately ±0.02 (or less than 1% for a $C_{l,max}$ value of 4.5). Repeatability studies confirmed this level.

Drag data were computed by integration of the static and total pressures obtained from the LTPT wake survey system. The wake profiles were measured with a five-hole-probe rake located 1.35c downstream of the model. The five-hole pressure probes were calibrated with respect to total pressure, static pressure, and flow pitch angle over a range of pitch angles from -30 to 30 deg. On the basis of the spanwise C_p distributions and a preliminary wake profile study that covered the center 44% of the model span, the flows were determined to be mostly two dimensional. Hence, the wake profile data were taken only at the centerline station. Integration of the local wake profile yielded the drag data presented here. Again, using the Kline and McClintock method,[10] the uncertainty in C_d was calculated to be approximately ±0.0010 for the large wakes of high-lift models (e.g., 2.5% for a typical C_d value of 0.0400).[11] Repeatability studies also confirmed this level.

Four rows of streamlined brackets were needed to support the high-lift configuration (Fig. 5) that was a result of the very high loads developed at the high test pressures. As mentioned previously, the flow is substantially two dimensional along the model center span and the maximum spanwise variation in C_p near the maximum lift was only 0.05 in the region between the flap brackets. This, together with the fact that all lift and drag calculations were integrated from data taken along the model centerline, the furthest possible distance from the brackets, shows that the support brackets' influence on the results herein is believed to be negligible. The nomenclature defining the key geometric parameters of high-lift systems is shown in Fig. 6. All gap and overhang (OH) values in this paper are expressed in terms of percent of cruise chord %c (all high-lift components stowed).

High-Lift System Design

The new high-lift system was designed with the objective of achieving high levels of performance while maintaining attached flow on the single-segment flap at flight Reynolds numbers. The high-lift system was designed to achieve maximum-lift levels similar to the reference single-segment flap.[4] The structured-grid, incompressible Navier-Stokes code, INS2D,[6]

with the Baldwin-Barth turbulence model was used for the computational analysis of the NASA and reference airfoils. Although INS2D has some known limitations (i.e., incompressible), it was chosen for its speed and simplicity, these are important characteristics for a design code. Hence, a secondary goal of the present study was to find out how well the code performed as a design tool for high-lift airfoils.

For the new high-lift components, no variable (or mission adaptive) designs were considered. The new flap was similar in shape to the flap of Ref. 4. The flap was designed to have minimal flow separation at a 30-deg flap setting with no overlap between the flap leading edge and the spoiler trailing edge. INS2D predictions for the current NASA high-lift configuration indicated it would have improved performance compared to the Ref. 4 high-lift airfoil (Fig. 7). This predicted improvement is largely attributable to the increased (aft) camber of the NASA airfoil.

Experimental Results

The following discussion reviews highlights of the subject test results obtained in the LTPT. NASA Langley Research Center's cruise and high-lift airfoils were tested and the experimental results were compared to INS2D predictions, as well as to the results of their respective reference airfoil counterparts. Effects of varying the slat and flap gaps and overhangs of the NASA airfoil were investigated experimentally. Unless otherwise stated, the experiments were conducted at a Mach number of 0.20. The Re_c of 4.2, 9, and 16 x 10^6 were achieved by pressurizing the wind tunnel to 1.8, 3.7, and 6.5 atm, respectively.

Computational Validation

As stated previously, the NASA cruise airfoil does have increased thickness and aft camber (see Figs. 2 and 3) that will allow it to generate more lift than the Ref. 2 cruise airfoil. The INS2D predictions indicated that the NASA cruise airfoil would produce more lift than the reference airfoil at all angles of attack (Fig. 8). The experimental data in the same figure validate most of that, except near $C_{l,max}$. The additional camber (as compared to the reference airfoil) increased the

loading over the entire airfoil (Fig. 9). INS2D's predictions for the lift are in excellent agreement with experimental data for angles of attack up to 10 deg. However, INS2D did not accurately predict the stall angle (flow breakdown) of either airfoil. In addition, INS2D incorrectly predicted that the NASA airfoil would generate significantly higher $C_{l,max}$ than the reference airfoil. INS2D did not accurately predict the onset and severity of trailing-edge separation, as indicated by the sharp decrease in trailing-edge pressures shown in Fig. 10. Furthermore, INS2D did not correctly predict the qualitative differences in the stall types for the two airfoils. INS2D predicted both airfoils to exhibit a trailing-edge type stall, as indicated by the gradual rounding over of the lift curves at $C_{l,max}$ in Fig. 8. The NASA airfoil experimental results did exhibit this trailing-edge type stall. However, the reference airfoil experimental results exhibited more of a leading-edge type stall (normally characterized by the abrupt loss in lift after stall).

The initial multielement testing was performed with the slat overhang and gap set at -2.5 and 2.94%, respectively, and the flap overhang and gap set at 0 and 1.27%, respectively. These values were the design rigging for the three-element airfoil and are close to the optimum rigging of the reference airfoil.[4] As will be shown later, this rigging was very close to the best rigging (determined experimentally). A comparison of the experimental and INS2D predicted performance for the three-element airfoils is shown in Fig. 7. As can be seen the code did not accurately predict the performance of the two airfoils near $C_{l,max}$. INS2D does capture the differences in performance between the NASA and reference airfoils over a large portion of the angle-of-attack range below stall. Specifically, at an approach condition (~8-deg angle of attack), INS2D's prediction for the increased lift of the NASA airfoil relative to the reference airfoil is in good agreement with the experimentally observed increase. The difference between the experimental and INS2D results near the maximum lift may be, at least partially, attributed to the lack of boundary-layer transition simulation (computations were fully turbulent) and the possible compressibility effects near stall, where the flow over the slat could approach the sonic speed.

Leading-Edge Slat-Rigging Effects

For this portion of the study, the flap was set at 30-deg deflection with an overhang of 0% and a gap of 1.27%. The flap position was fixed, whereas the slat overhang and gap were varied. Starting with the design slat overhang of -2.5%, the overhang was moved ±1.0%, along with at least three gap changes for each overhang. The effect of Reynolds number on leading-edge slat-rigging effects is shown in Fig. 11. At the 4.2 x 10^6 Reynolds number, a gap size in the range of 2-3% produced about the same level of $C_{l,max}$ at around 4.5, independent of the overhang examined. To ensure this conclusion was correct, a fourth overhang of -2.0% was tried with a gap of 2.52%, and the result was consistent with the finding (see Fig. 11). Within the range of experimental uncertainty (±0.02), the best position (highest $C_{l,max}$) seems to also be the design rigging with a slat overhang of -2.5% and a slat gap of 2.94%. The 4.2 x 10^6 Reynolds number is a typical chord Reynolds number for many full-span, three-dimensional, low-speed wind-tunnel tests. The maximum-lift value realized for the airfoil in this test is highest at the lower Reynolds number. Thus, rigging the slat based on low Reynolds number testing would lead the designer to chose a rigging that is clearly not optimal at the higher Reynolds numbers. The best slat rigging for this study was at an overhang of -1.5% and a gap of 2.44% (Fig. 11). This result is repeatable and the data falls outside the $C_{l,max}$ uncertainty of ±0.02.

In examining the results shown in Fig. 11, it can be seen for the -2.5% overhang case the effect of gap on maximum lift is clearly Reynolds number dependent. When the slat gap is increased from 2.94% to 3.27%, there was a sharp decrease in the maximum-lift coefficient for Reynolds numbers of 4.2 and 9 x 10^6, respectively. However, at the highest Reynolds number, the maximum-lift level remains essentially unchanged for the three gaps tested. The effects of slat gap on the lift curves for 9 and 16 x 10^6 Reynolds numbers are shown in Figs. 12 and 13, respectively, for the -2.5% overhang. At 9 x 10^6 Reynolds number, increasing the gap from 2.94 to 3.27% reduces the loading on the main element by reducing its suction peak, as shown in Fig. 14 for an angle of attack just below stall ($\alpha = 20°$). However, at 16 x 10^6 Reynolds number, the

main-element (and total) loading does not change appreciably, as illustrated in Figs. 13 and 15. This could be caused by the boundary-layer/wakes becoming thinner as Reynolds number increased, decreasing the gap sensitivity of the main element (for the gaps tested at this overhang).

From Figs. 12 and 13, it can be seen that changing the slat gap clearly influences the main-element loading, and secondarily influences the slat loading. For the increase in slat gap from 2.94 to 3.27% shown in Fig. 12, there is a noticeable decrease in the main-element (and slat) loading at the higher angles of attack because of the reduced suction peak. From these results it can be inferred that the change in performance is caused primarily by changes in the main-element loading. The reduction in main-element's suction peak led to a corresponding reduction in the slat lift in the form of a reduced aft loading. Thus, a change in slat gap (for a constant overhang) acts on the main element, and the main-element loading influences slat and flap loading. In comparison, the slat deflection study of Ref. 2 showed a change in slat deflection (angle of attack) acts primarily on the slat itself, and the main-element and flap loadings are secondarily impacted (the main-element loading does decrease as the slat loading increased). The difference between the two studies is probably because the slat gap change of the current study primarily affects the slat's wake flow (and its effect) over the main element; whereas the slat gap and deflection changes of Ref. 2 primarily affects the slat's own circulation and suction peak.

Trailing-Edge Flap-Rigging Effects

For this portion of the study, the slat position was fixed at the best location as determined from the previous study, i.e. an overhang of -1.5% and a gap of 2.44%. The flap deflection was fixed at 30 deg, and its overhang and gap were varied. The effect of Reynolds number on trailing-edge flap-rigging effects is shown in Fig. 16. The effect of Fowler motion (extending the effective chord of the high-lift system) on $C_{l,max}$ is prevalent in Fig. 16. As the overhang becomes more negative (no overlap), the maximum-lift values steadily increase.

Despite the high $C_{l,max}$ produced by a more negative overhang, it was discovered that flow separation occurred on the flap for all the cases that had a larger negative overhang (i.e., -0.5 and -

1.0%). For example, a typical effect of large negative overhang on flap performance is shown in Fig. 17. It can be observed that the lift is significantly reduced and the drag drastically increased when the overhang is increased to -1.0%. This is caused by the massive separation on the flap, as shown in the pressure distributions of Fig. 18. This massive separation on the flap can have a global effect on the flow over the upper surfaces of the entire high-lift system. The separation reduced the flap loading as well as the upwash (from the flap) on the main element and slat, thereby reducing their respective loading (Fig. 18). As the angle of attack is increased, the flap effective angle of attack is reduced because of the increased wake spreading from the forward elements. At α = 20 deg, the flap angle of attack is reduced sufficiently to reattach the flow, increasing the loading on the flap and consequently the main element (from the increased upwash from the flap), and thus the total loading (Fig. 19). This demonstrates the importance of keeping the flow attached on the flap, since the lift generated at an approach condition (8 deg) is significantly reduced (and the drag is significantly increased) for the separated case, even though the $C_{l,max}$ values are almost identical.

For the design of a typical high-lift system, the optimum point was a compromise of maximum lift and minimum flow separation (drag) at an approach-type condition. In the current case, the best flap gap and overhang tested was a gap of 1.47% and an overhang of -0.25%. These values are very close to the design values of gap and overhang (1.27 and 0%, respectively).

Reynolds and Mach Number Effects

The Reynolds and Mach number effects on the best configuration are shown in Figs. 20 and 21, respectively. As can be seen in Fig. 20, the lift is almost identical and well behaved for chord Reynolds numbers of 9 and 16 x 10^6. However, there is a slight difference between these lift curves and that of the 4.2 x 10^6 case at approach conditions. This difference is a result of the flow separation that occurred on the flap between 4- and 14-deg angle of attack at the lower (nonflight scale) Reynolds number. Similar to results reported in Refs. 2-4, the measured maximum-lift levels of Fig. 21 exhibit a significant dependence on Mach number at a given chord Reynolds

number of 9 x 10^6. The (expected) compressibility effect at $M_\infty = 0.26$ limited the slat suction peak (see Fig. 22) and caused the stall to occur at a lower angle of attack as compared to the 0.15 and 0.20 Mach number results. The peak Mach number on the slat (at all freestream Mach numbers tested) significantly exceeded sonic values. The critical (sonic) C_p for $M_\infty = 0.26$ is about -9.4. As can be seen in Fig. 22, the $C_{p,max}$ on the slat is much greater than this value.

Conclusions

New high-lift airfoil components have been designed using INS2D for the NASA EET high-lift research airfoil. The new components have been tested in the NASA Langley Research Center's Low-Turbulence Pressure Tunnel and the effects of Reynolds number and Mach number on performance have been studied. Several salient conclusions can be drawn from this work.

1) The structured-grid Navier-Stokes method INS2D accurately predicted the lift and performance difference of the NASA and reference airfoils at approach conditions for the single-element (cruise) and three-element (high-lift) airfoils. However, INS2D using the one-equation Baldwin-Barth turbulence model did not accurately predict the experimentally observed maximum-lift values of either airfoil.
2) Significant Reynolds number effects were observed on the leading- and trailing-edge rigging effects. The maximum-lift values decreased as Reynolds number increased for the leading-edge rigging studied. The sensitivity to gap was also Reynolds-number dependent for some of the slat (and flap) overhangs tested.
3) Separation occurred on the single-segment flap for the negative-overhang cases tested in this study. This is especially important since a separated flap generates increased drag (and associated noise and vibration), and possibly less total lift than the best flap with attached flow at an approach condition.

While the present work has increased the existing database of leading- and trailing-edge rigging effects, it is apparent that more detailed work is needed. Specifically, studying the slat wake and

main element interaction in more detail is necessary to understand the possible implications for high-lift system improvement. Also, an improved understanding of the boundary-layer transition process on each of the elements as a function of Reynolds number is urgently needed to determine how to properly simulate full-scale conditions on three-dimentional high-lift systems. And, finally, much work is needed to develop turbulence models that better represent multielement airfoil flows to increase the role/effectiveness of computational fluid dynamics in the design process.

Acknowledgments

This work was done under contract number NAS1-18763. The design of the high-lift components used for this paper was done by the Advanced Transport Aircraft Development segment of McDonnell Douglas Aerospace.

References

[1]Fidders, S. P., Kirby, D. A., Woodward, D. S., and Peckham, D. H., "Investigation Into the Effects of Scale and Compressibility on Lift and Drag in the RAE 5m Pressurized Low-Speed Wind Tunnel," *Aeronautical Journal*, Paper No. 1302, March 1985.

[2]Valarezo, W. O., Dominik, C. J., McGhee, R. J., Goodman, W. L., and Paschal, K. B., "Multi-Element Airfoil Optimization at High Reynolds Numbers," AIAA Paper No. 91-3332, September 1991.

[3]Valarezo, W. O., Dominik, C. J., and McGhee, R. J., "Reynolds and Mach Number Effects on Multielement Airfoils," Fifth Symposium on Numerical and Physical Aspects of Aerodynamic Flows, California State University, Long Beach, January 1992.

[4]Valarezo, W. O., Dominik, C. J., and McGhee, R. J., "High Reynolds Number Configuration Development of a High-Lift Airfoil," AGARD CP-515, Paper No. 10, 71st AGARD FDP Symposium on High-Lift System Aerodynamics, Banff, Alberta, October 1992.

[5]Morgan, H. L., Jr., "Model Geometry Description and Pressure Distribution Data from Tests of EET High-Lift Research Model Equipped with Full-Span Slat and Part-Span Flaps," NASA TM-80048, February 1979.

[6]Rogers, S. E., Wiltberger, N. L., and Kwak, D., "Efficient Simulation of Incompressible Viscous Flow Over Single and Multi-Element Airfoils," AIAA Paper 92-0405, January 1992.

[7]McGhee, R. J., Beasley, W. D., and Foster, J. M., "Recent Modifications and Calibration of the Langley Low-Turbulence-Pressure-Tunnel," NASA TP-2328, July 1984.

[8]Paschal, K., Goodman, W., McGhee, R., Walker, B., and Wilcox, P., "Evaluation of Tunnel Sidewall Boundary-Layer-Control Systems for High-Lift Airfoil Testing," AIAA Paper No. 91-3243, September 1991.

[9]Wlezien, R. W., Spencer, S. A., and Grubb, J. P., "Comparison of Flow Quality in Subsonic Pressure Tunnels," AIAA Paper No. 94-2503, June 1994.

[10]Kline, S. J. and McClintock F. A., “Describing Uncertainties in Single-Sample Experiments,” *Mechanical Engineering*, Jan. 1953, pp. 3-8.

[11]Friedman, I. P., “Calibration and Application of a New Wake Rake System for Drag Measurement of High Lift Airfoil Models,” M.S. Thesis, George Washington Univ., April 1991.

List of Figures

Fig. 15 Effect of slat gap on surface pressures ($M_\infty = 0.20$, $Re_c = 16 \times 10^6$, slat OH = -2.5%, α = 20 deg).

Fig. 16 Effect of Reynolds number on trailing-edge flap optimization ($M_\infty = 0.20$).

Fig. 17 Effect of flap overhang on lift and drag ($M_\infty = 0.20$, $Re_c = 16 \times 10^6$).

Fig. 18 Effect of flap overhang on surface pressures ($M_\infty = 0.20$, $Re_c = 16 \times 10^6$, $\alpha = 8$ deg).

Fig. 19 Effect of flap overhang on surface pressures ($M_\infty = 0.20$, $Re_c = 16 \times 10^6$, $\alpha = 20$ deg).

Fig. 20 Effect of Reynolds number on lift curves of optimum configuration ($M_\infty = 0.20$).

Fig. 21 Effect of Mach number on lift curves of optimum configuration ($Re_c = 9 \times 10^6$).

Fig. 22 Effect of Mach number on suction-peak pressures of optimum configuration ($Re_c = 9 \times 10^6$).

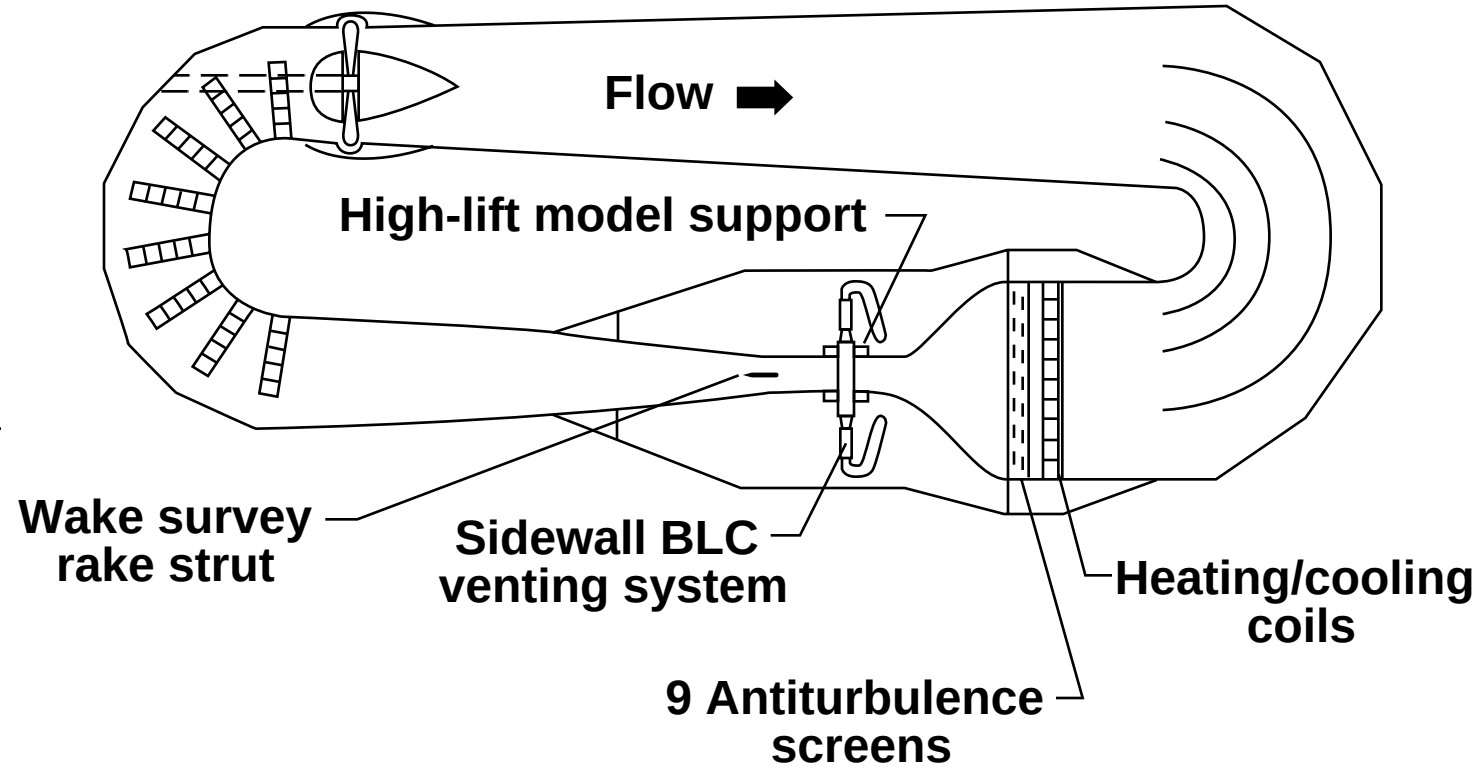

Fig. 1 NASA Langley Research Center's LTPT.

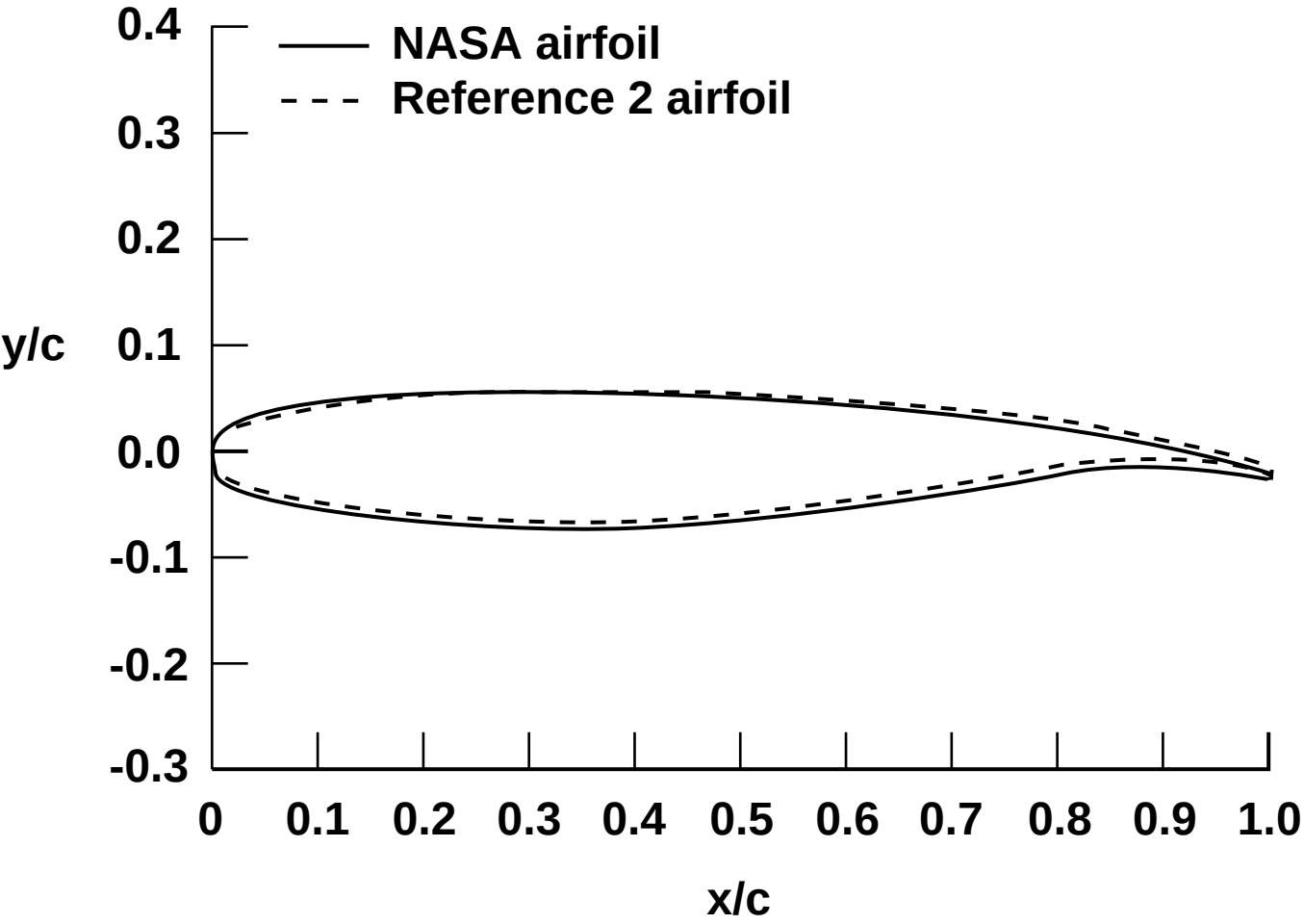

Fig. 2 Comparison of the cruise geometry between the NASA and reference airfoils.

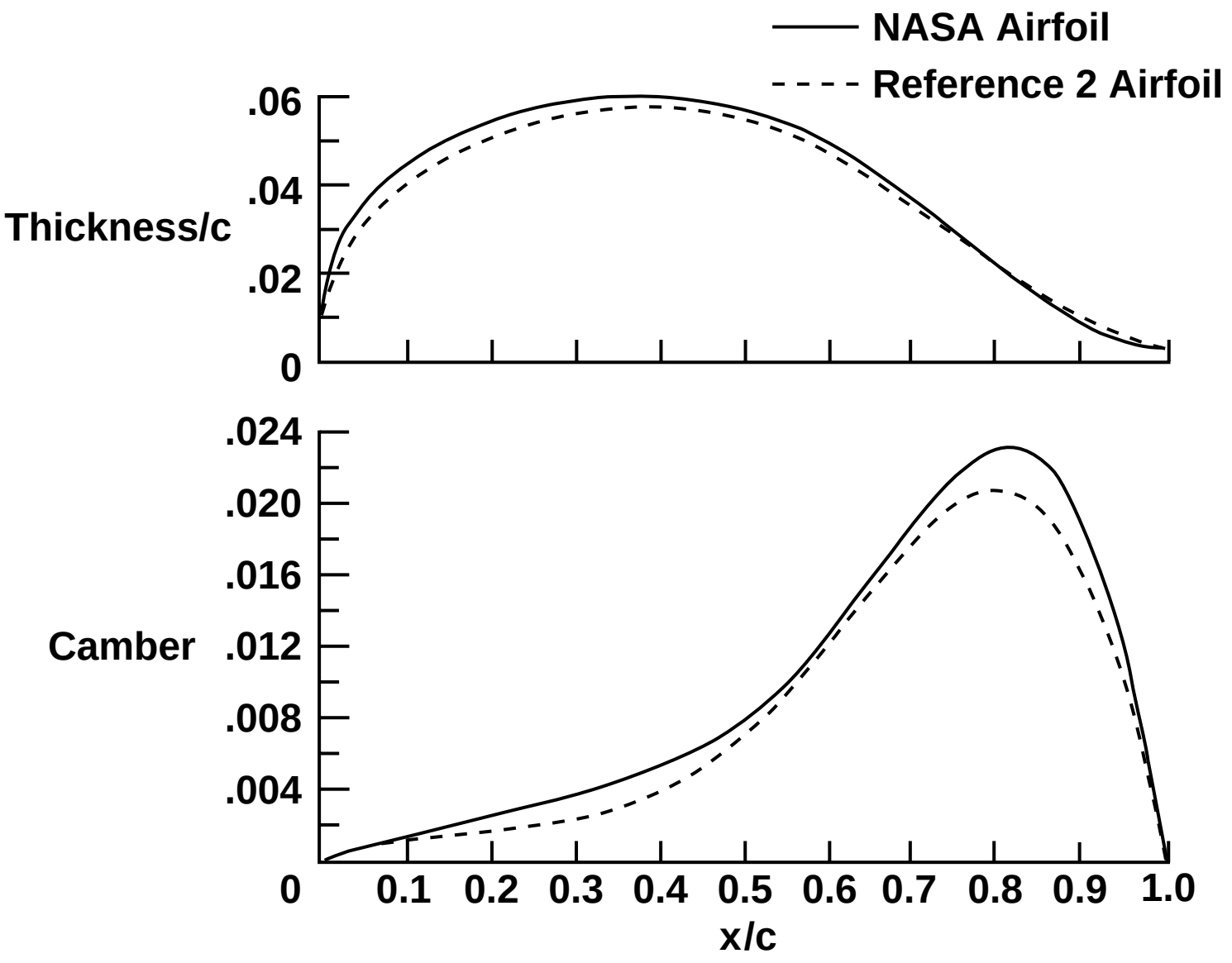

Fig. 3 Comparison of the thickness and camber distributions between the NASA and reference airfoils.

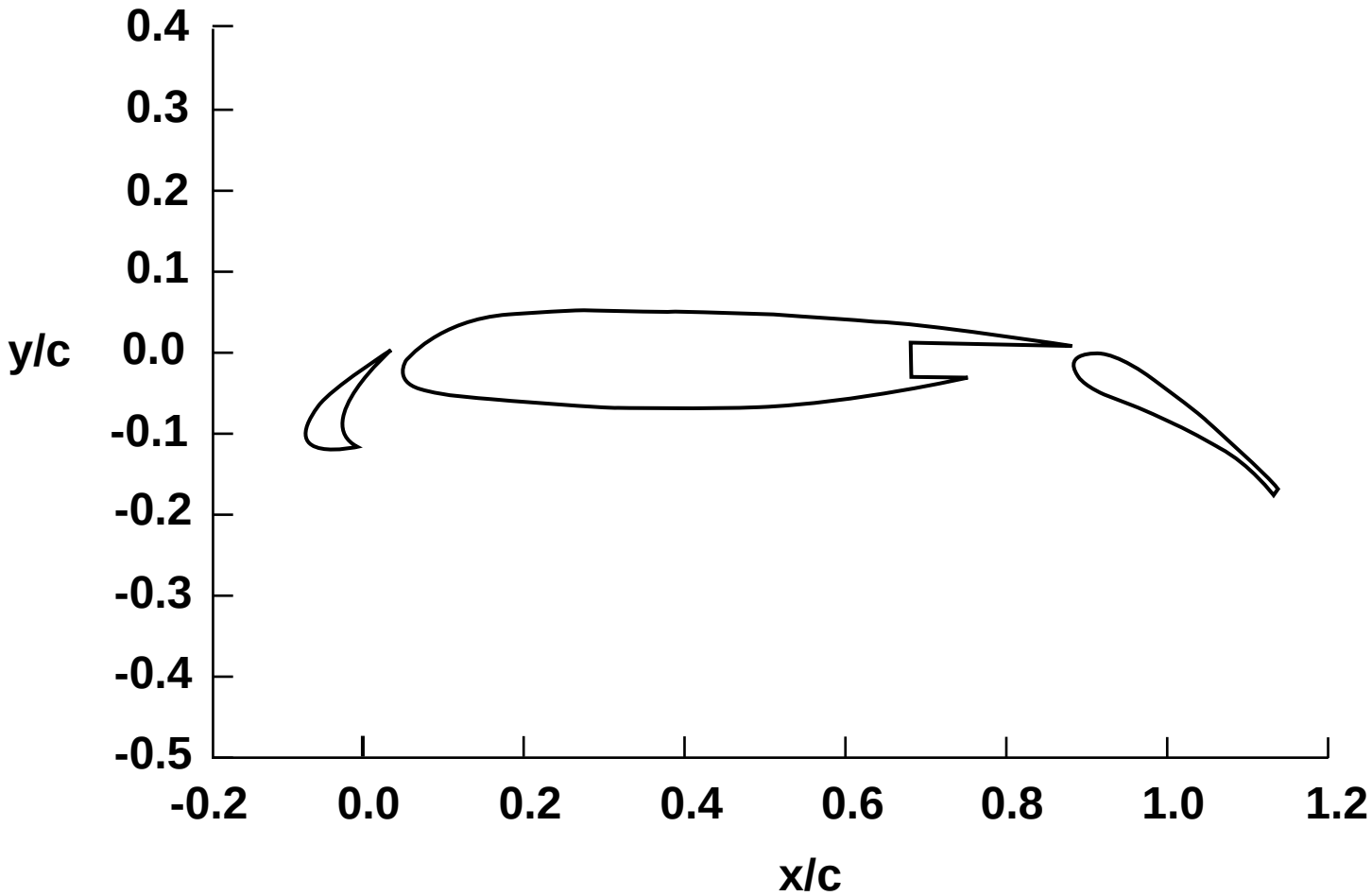

Fig. 4 Geometry of the NASA high-lift research airfoil.

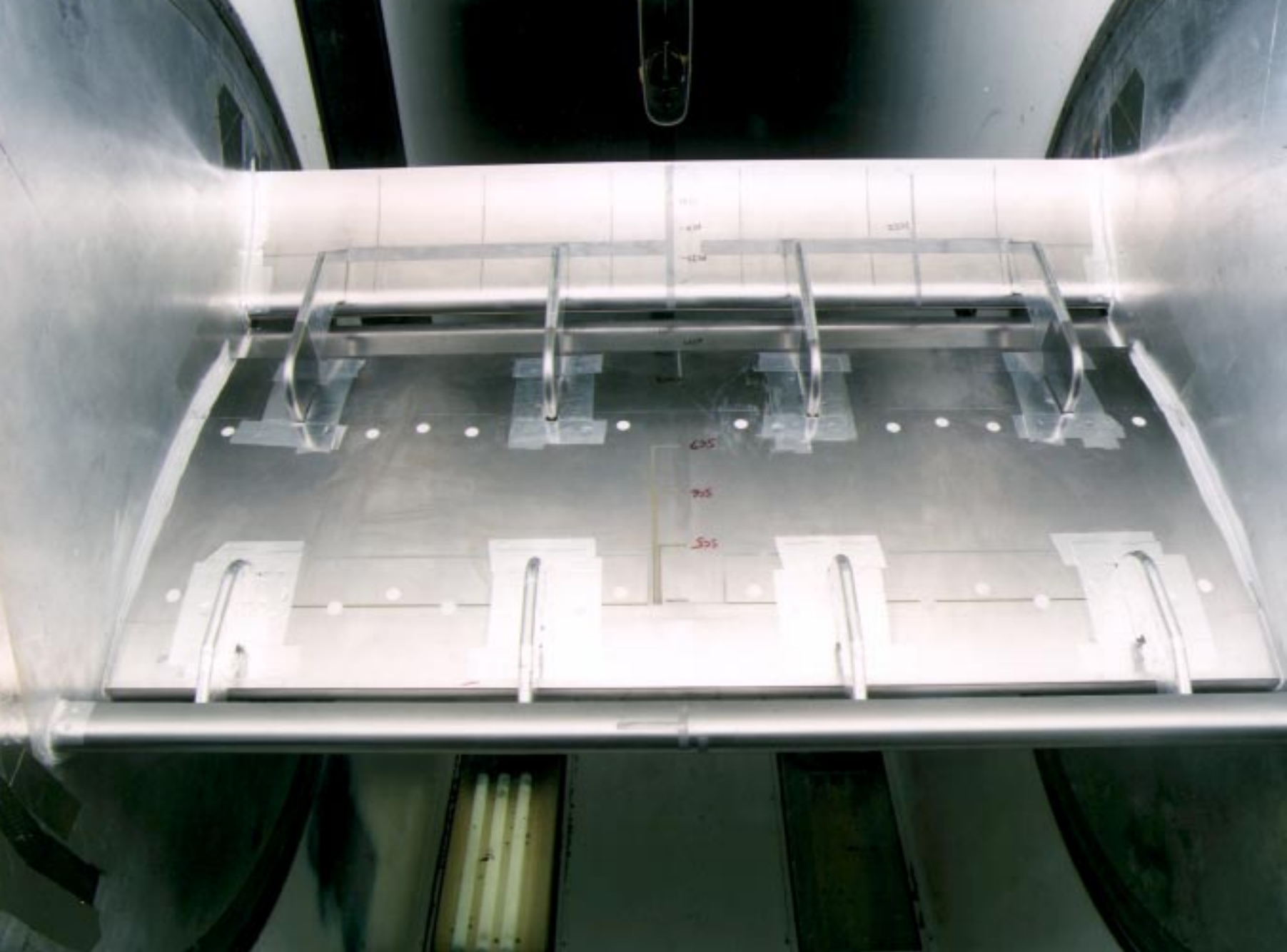

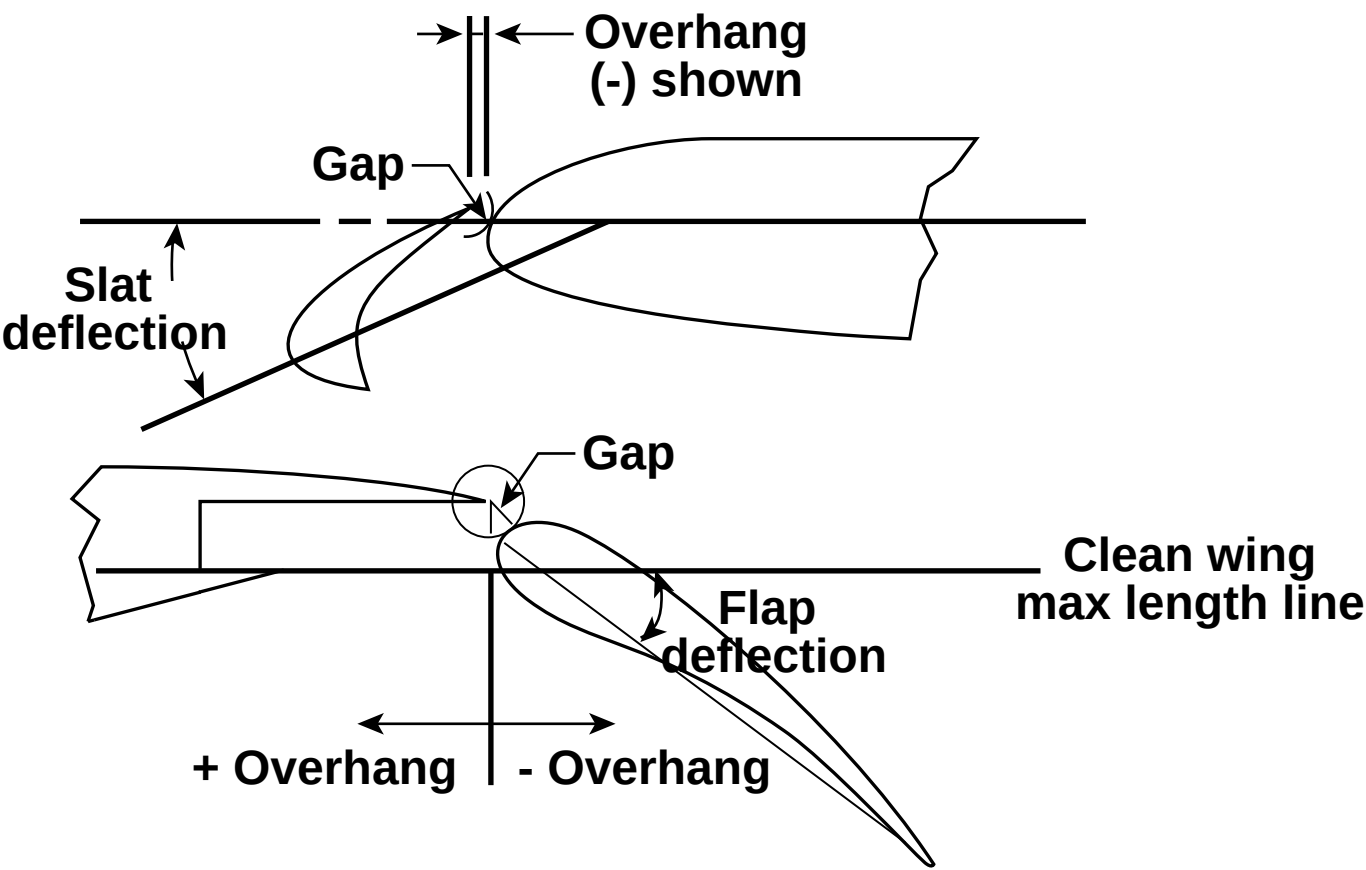

Fig. 6 Nomenclature for multielement airfoils.

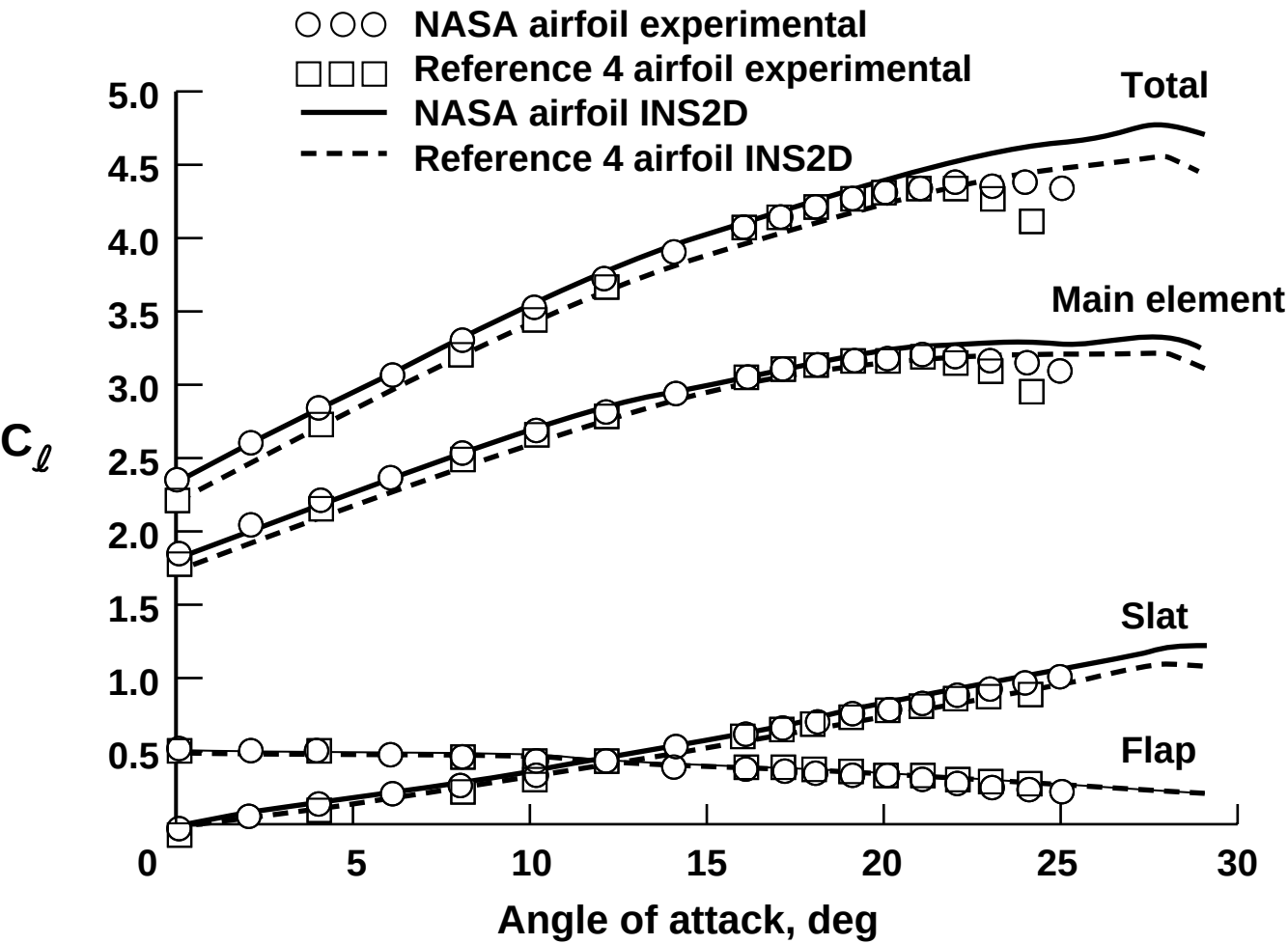

Fig. 7 Comparison between experimental and INS2D predicted performance of the NASA and reference high-lift airfoils (Mach No. = 0.20, Reynolds No. = 9 million).

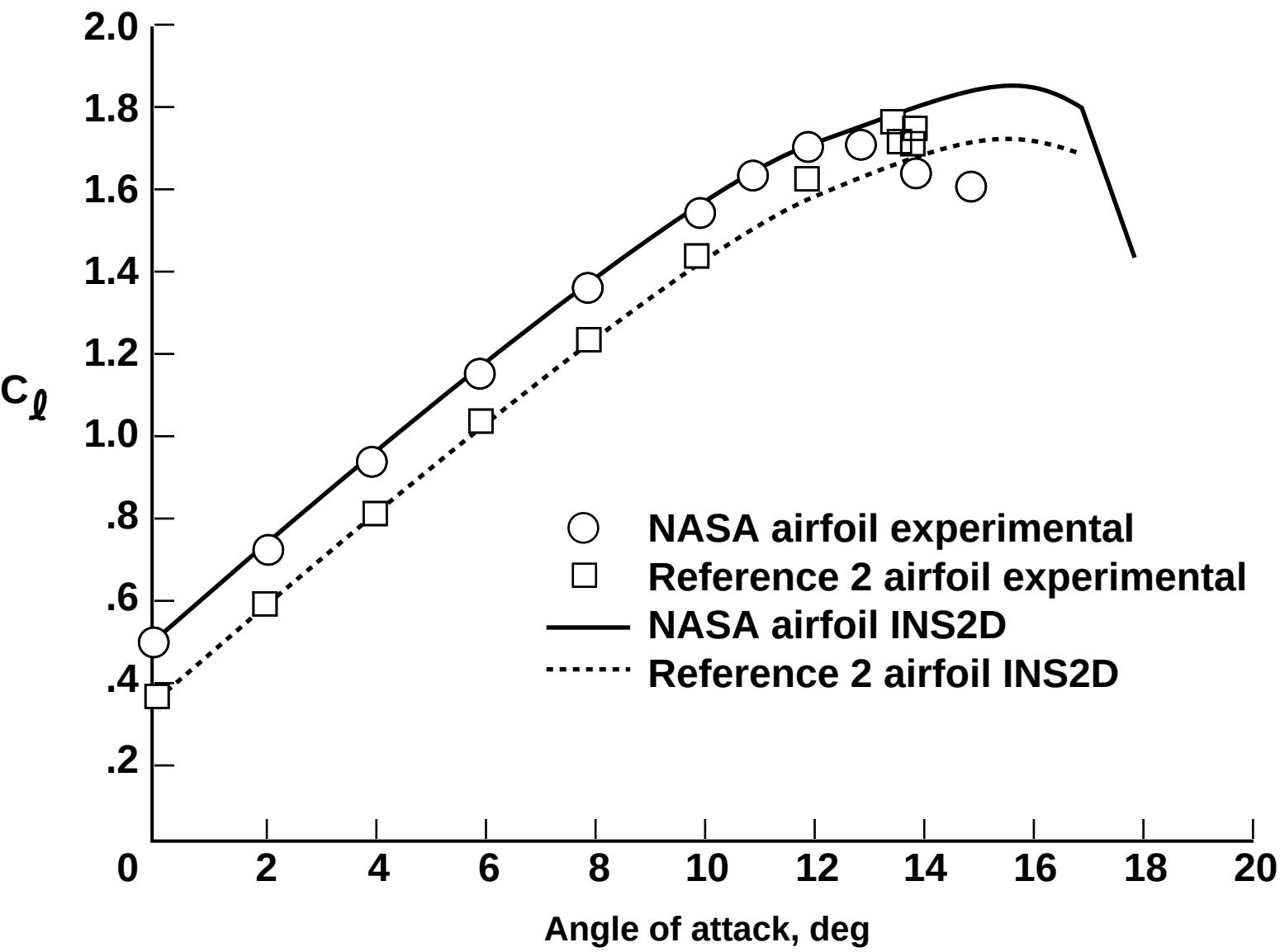

Fig. 8 Comparison between experimental and INS2D predicted performance of the NASA and reference cruise airfoils (Mach No. = 0.20, Reynolds No. = 9 million).

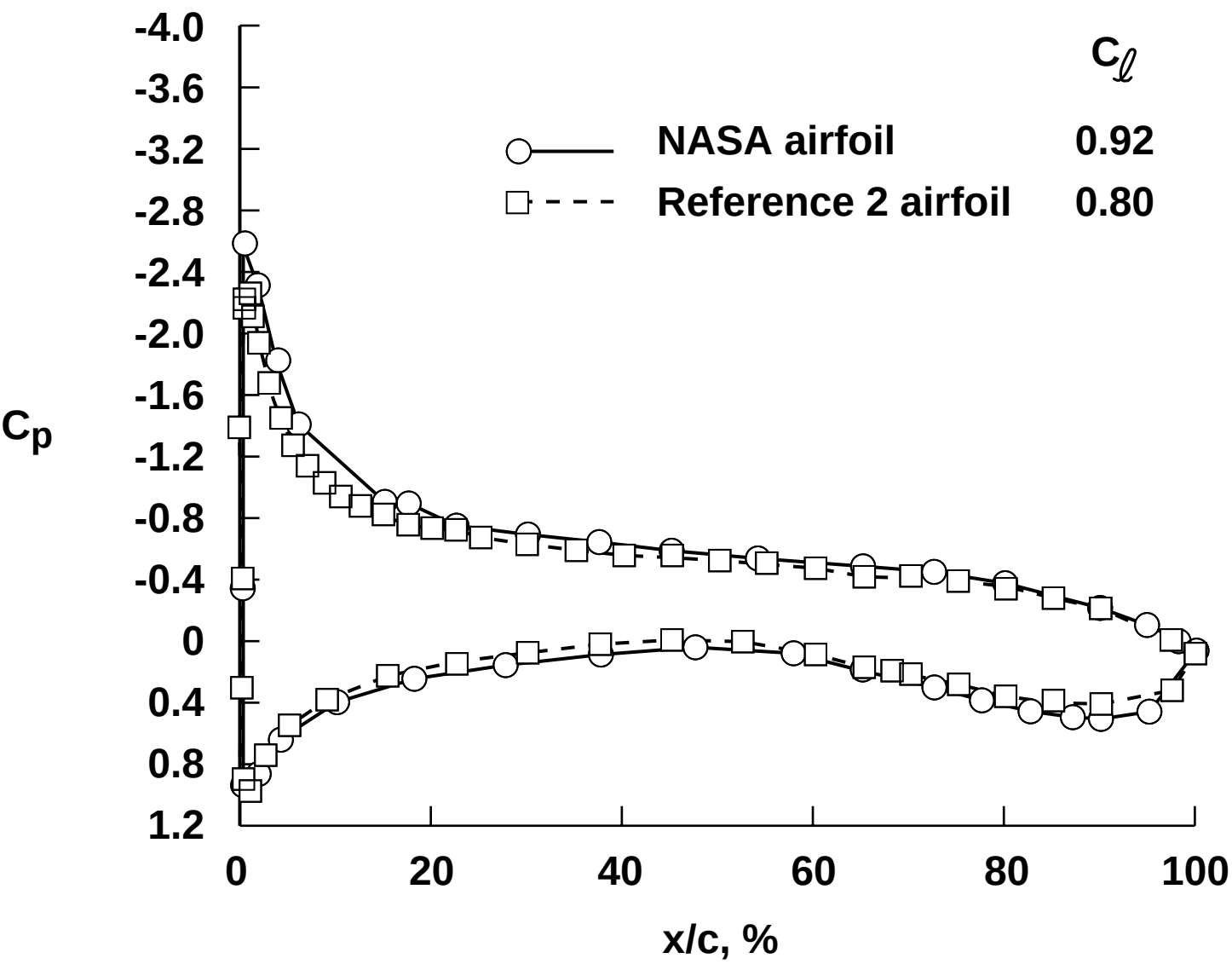

Fig. 9 Comparison of experimental pressure distributions for the NASA and reference cruise airfoils (Mach No. = 0.20, Reynolds No. = 9 million, angle of attack = 4 deg).

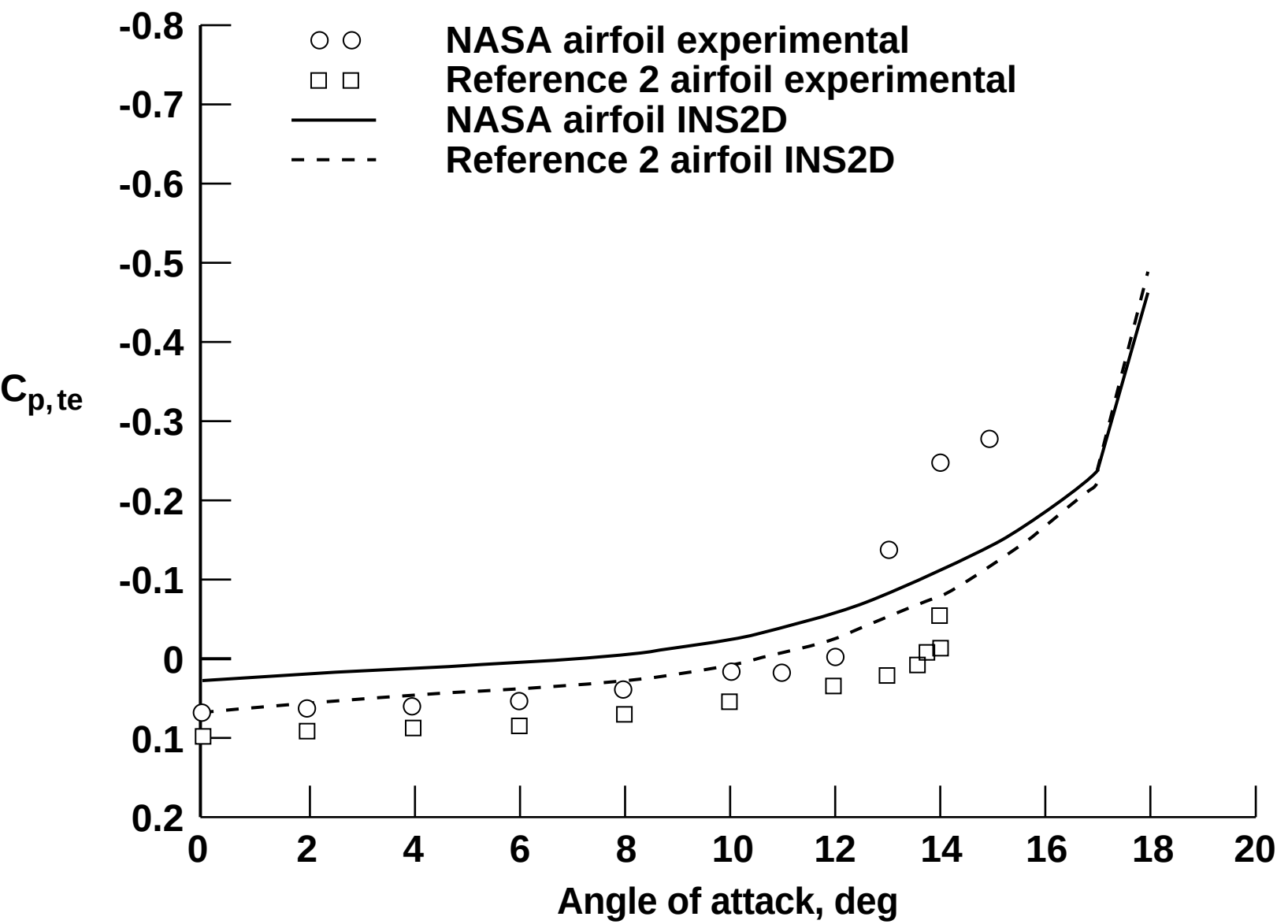

Fig. 10 Comparison between experimental and INS2D predicted trailing-edge pressures of the NASA and reference cruise airfoils (Mach No. = 0.20, Reynolds No. = 9 million).

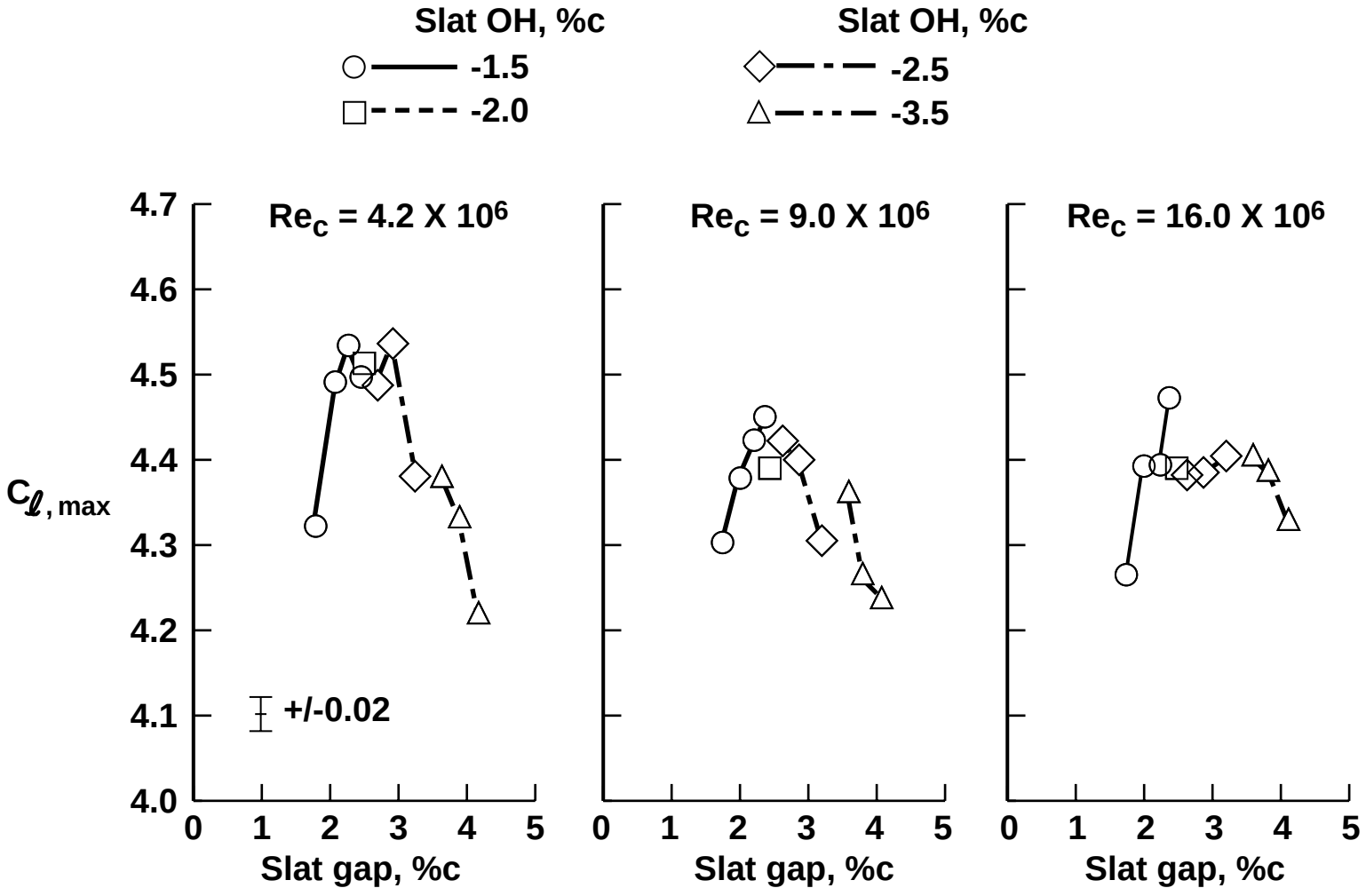

Fig. 11 Effect of Reynolds number on leading-edge slat optimization (Mach No. = 0.20).

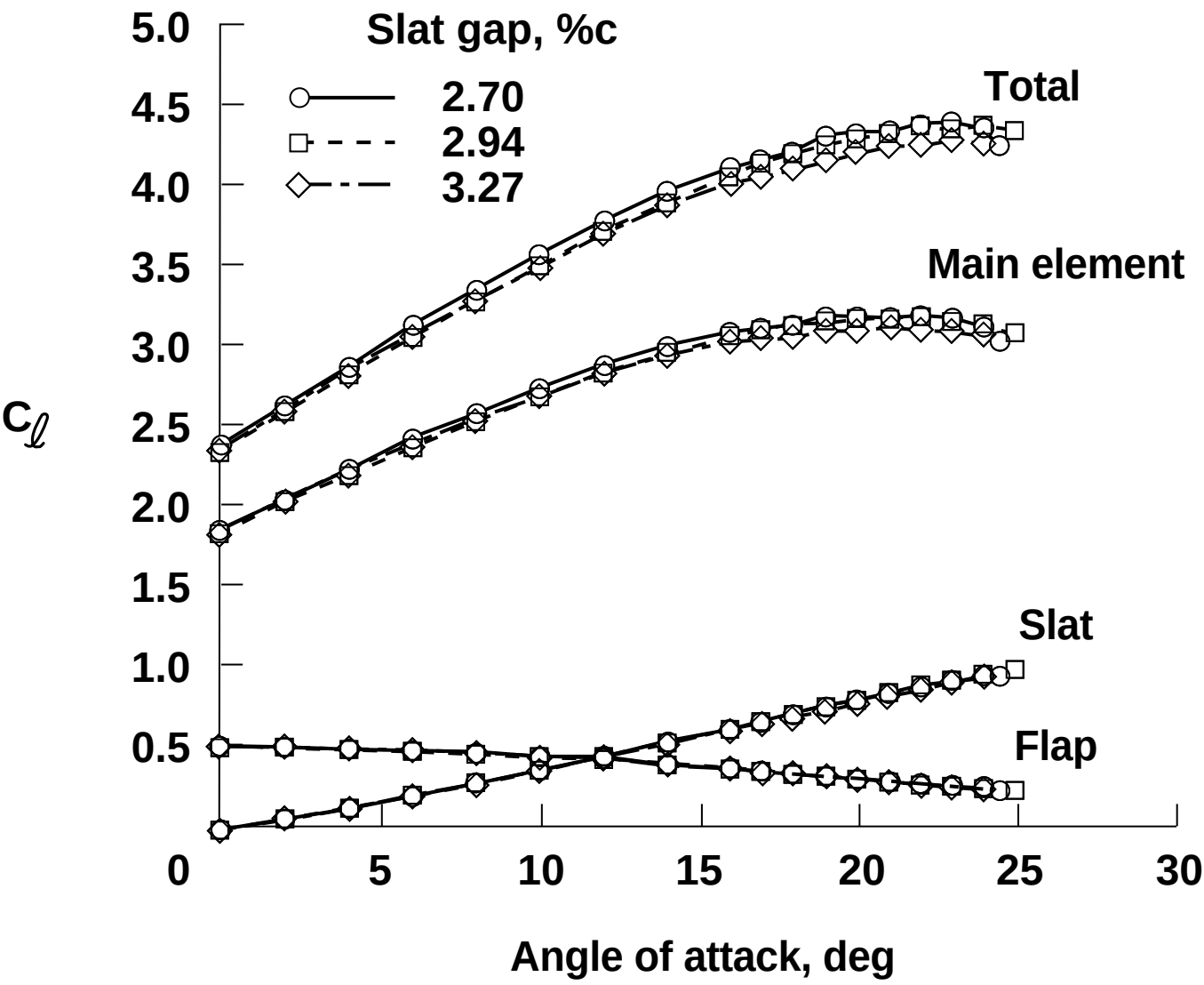

Fig. 12 Effect of slat gap on lift (Mach No. = 0.20, Reynolds No. = 9 million, slat OH = -2.5%).

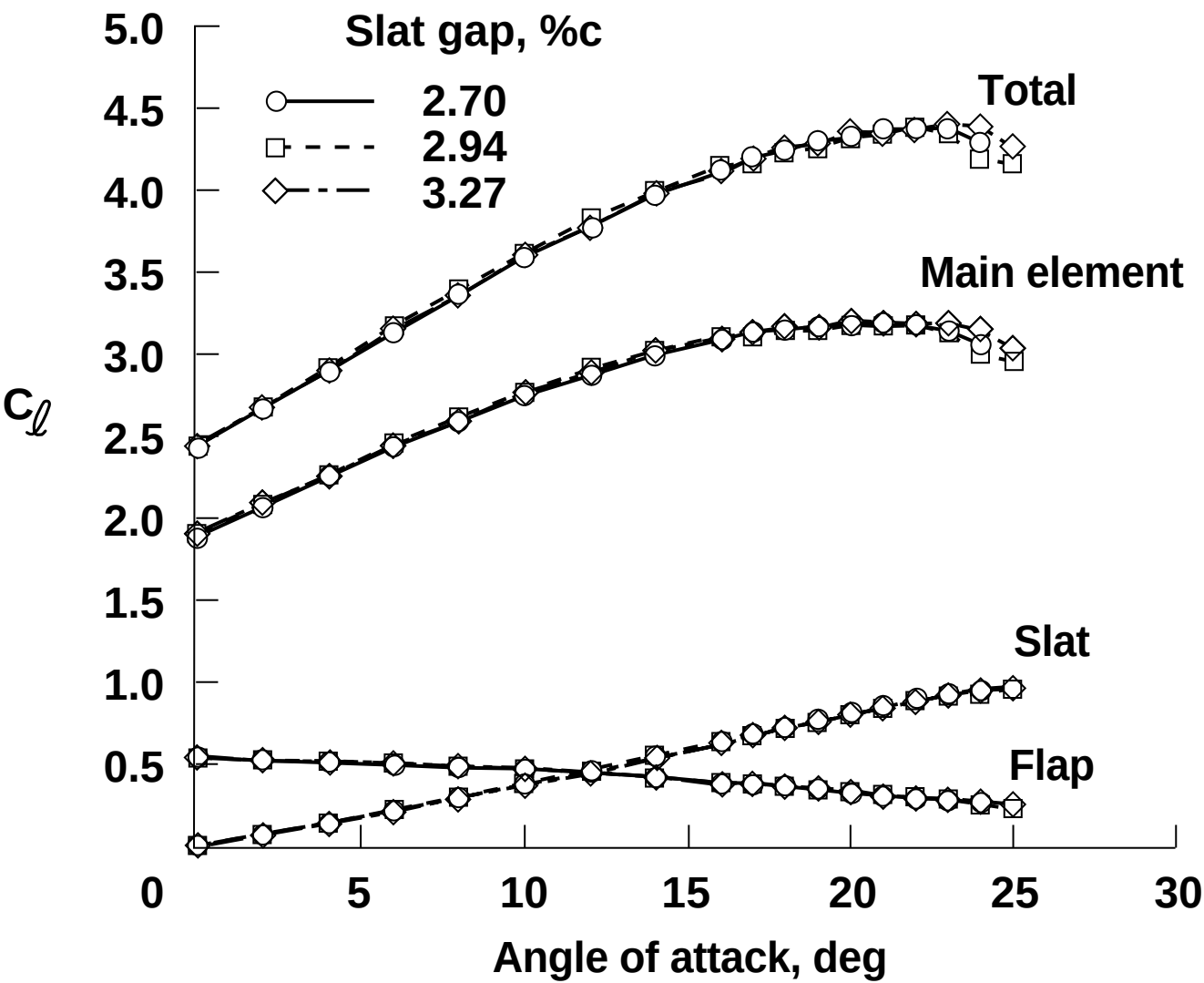

Fig. 13 Effect of slat gap on lift (Mach No. = 0.20, Reynolds No. = 16 million, slat OH = -2.5%).

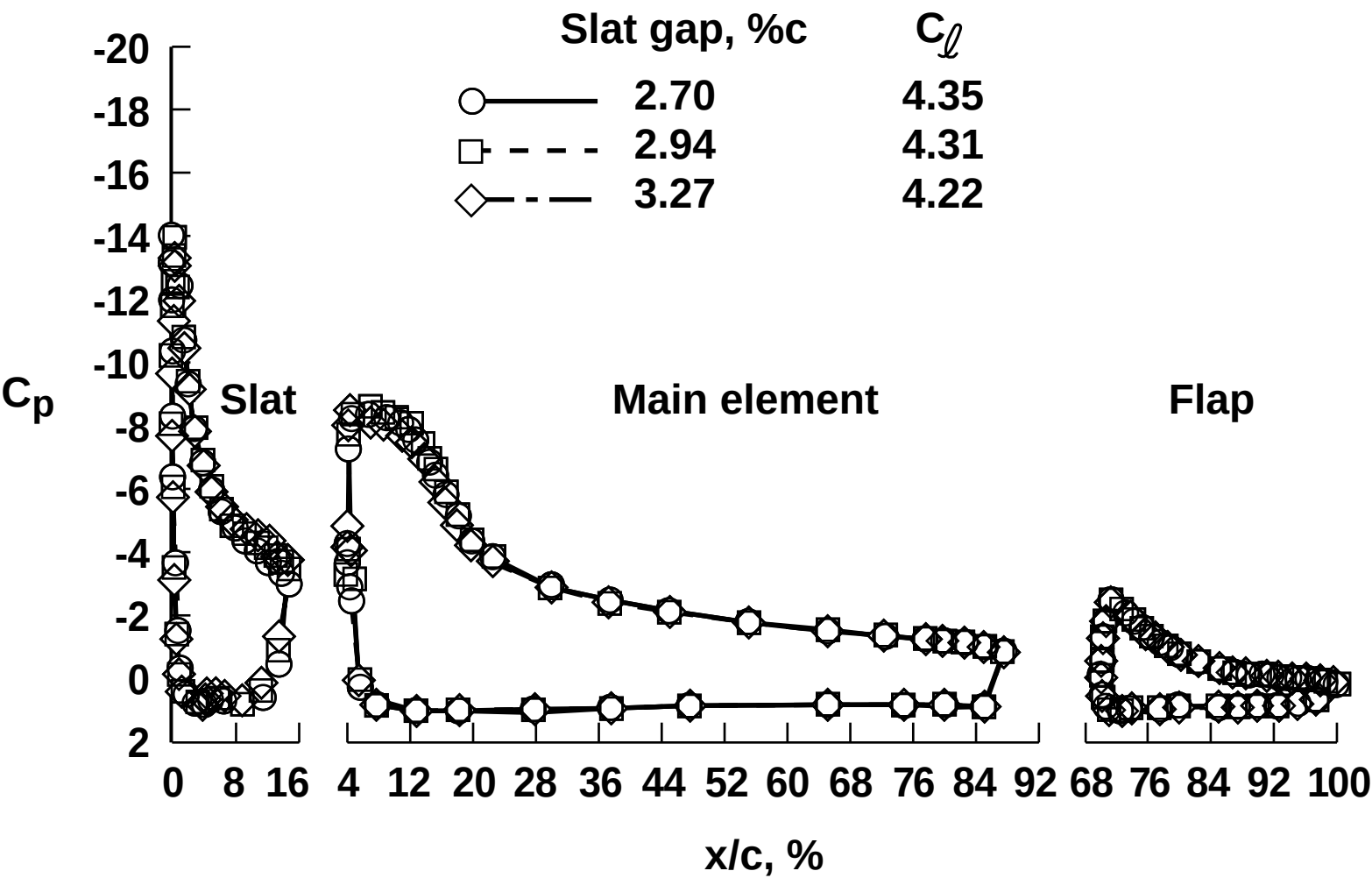

Fig. 14 Effect of slat gap on surface pressures (Mach No. = 0.20, Reynolds No. = 9 million, slat OH = -2.5%, angle of attack = 20 deg).

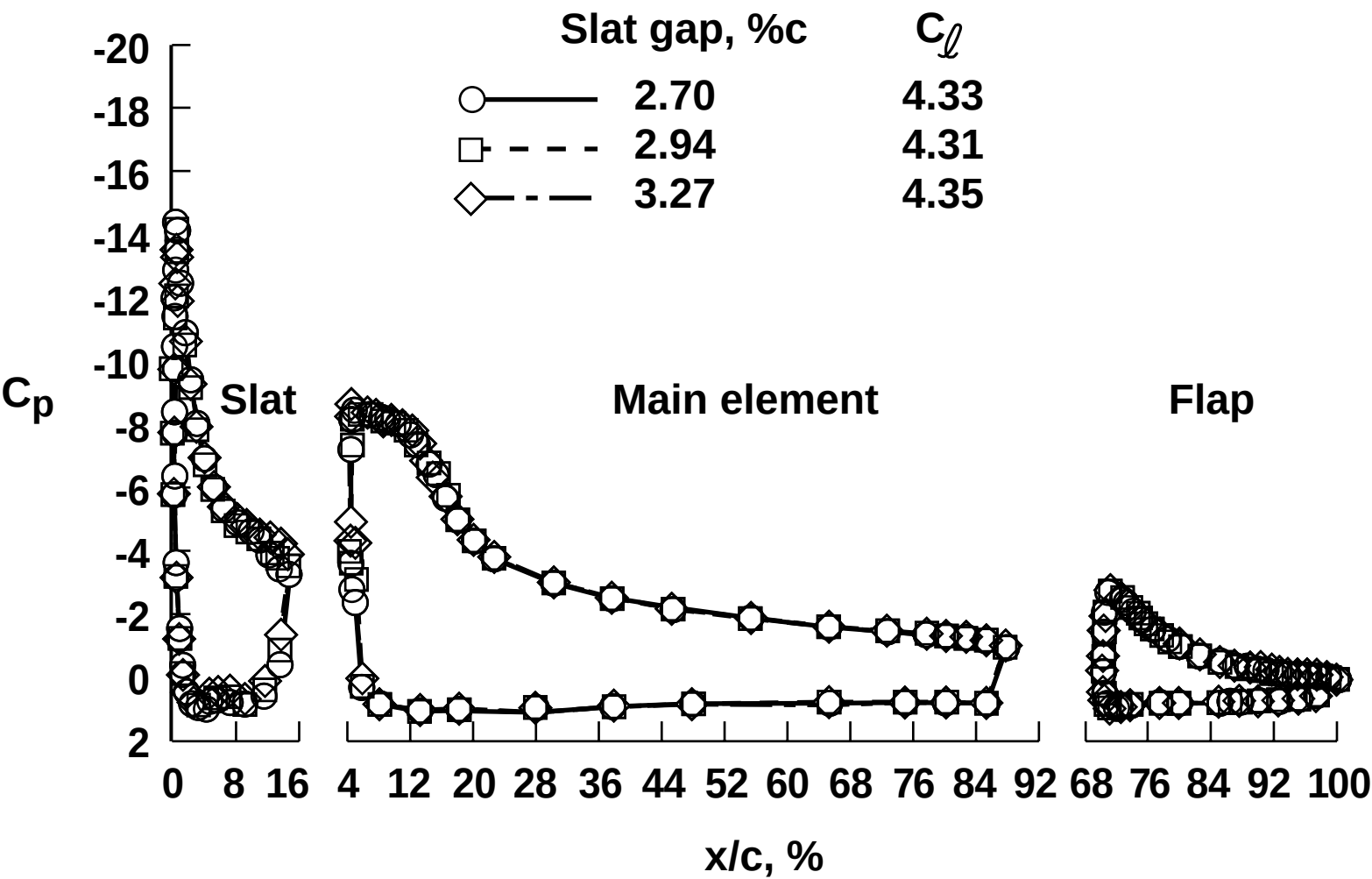

Fig. 15 Effect of slat gap on surface pressures (Mach No. = 0.20, Reynolds No. = 16 million, slat OH = -2.5%, angle of attack = 20 deg).

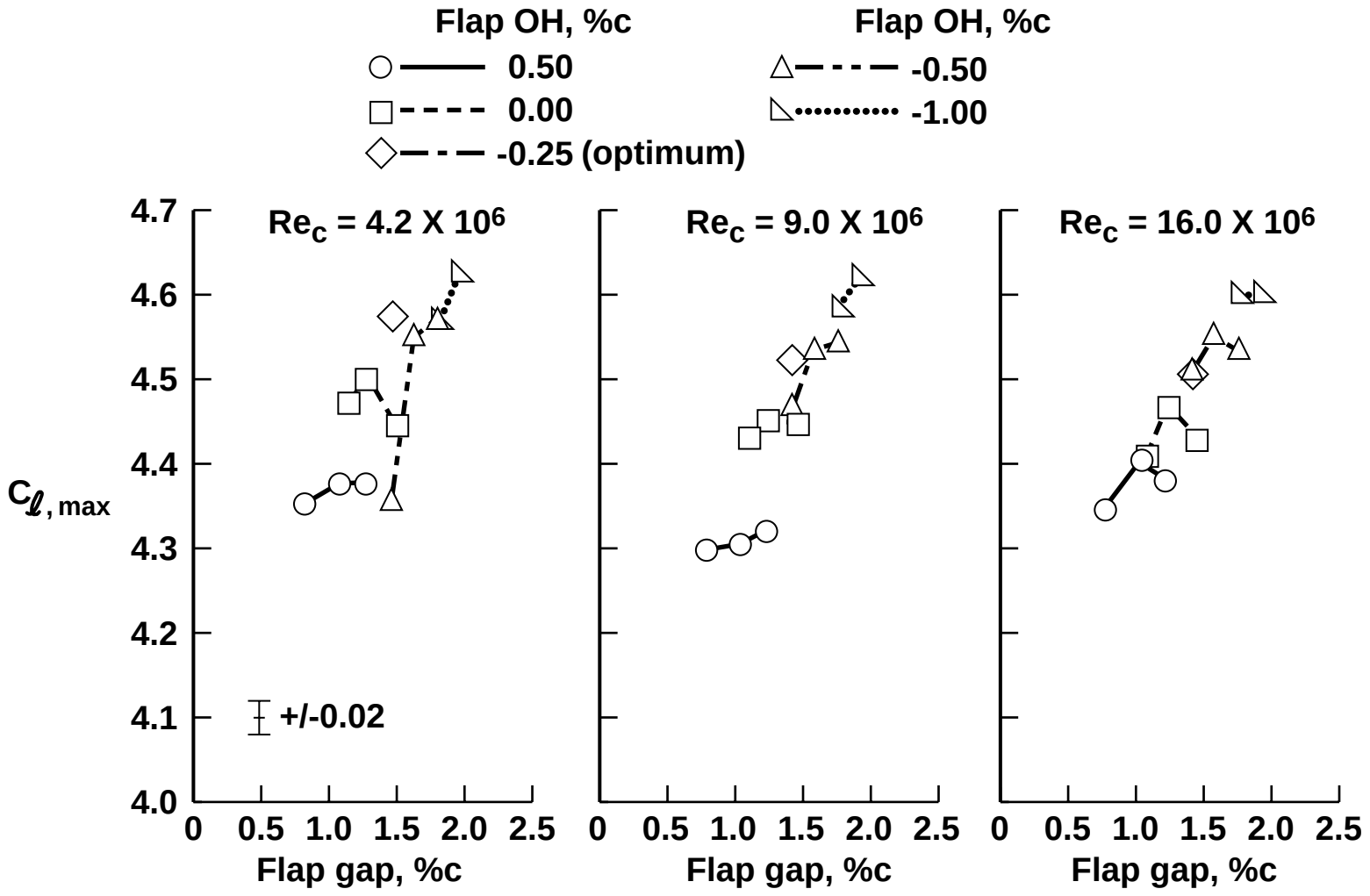

Fig. 16 Effect of Reynolds number on trailing-edge flap optimization (Mach No. = 0.20).

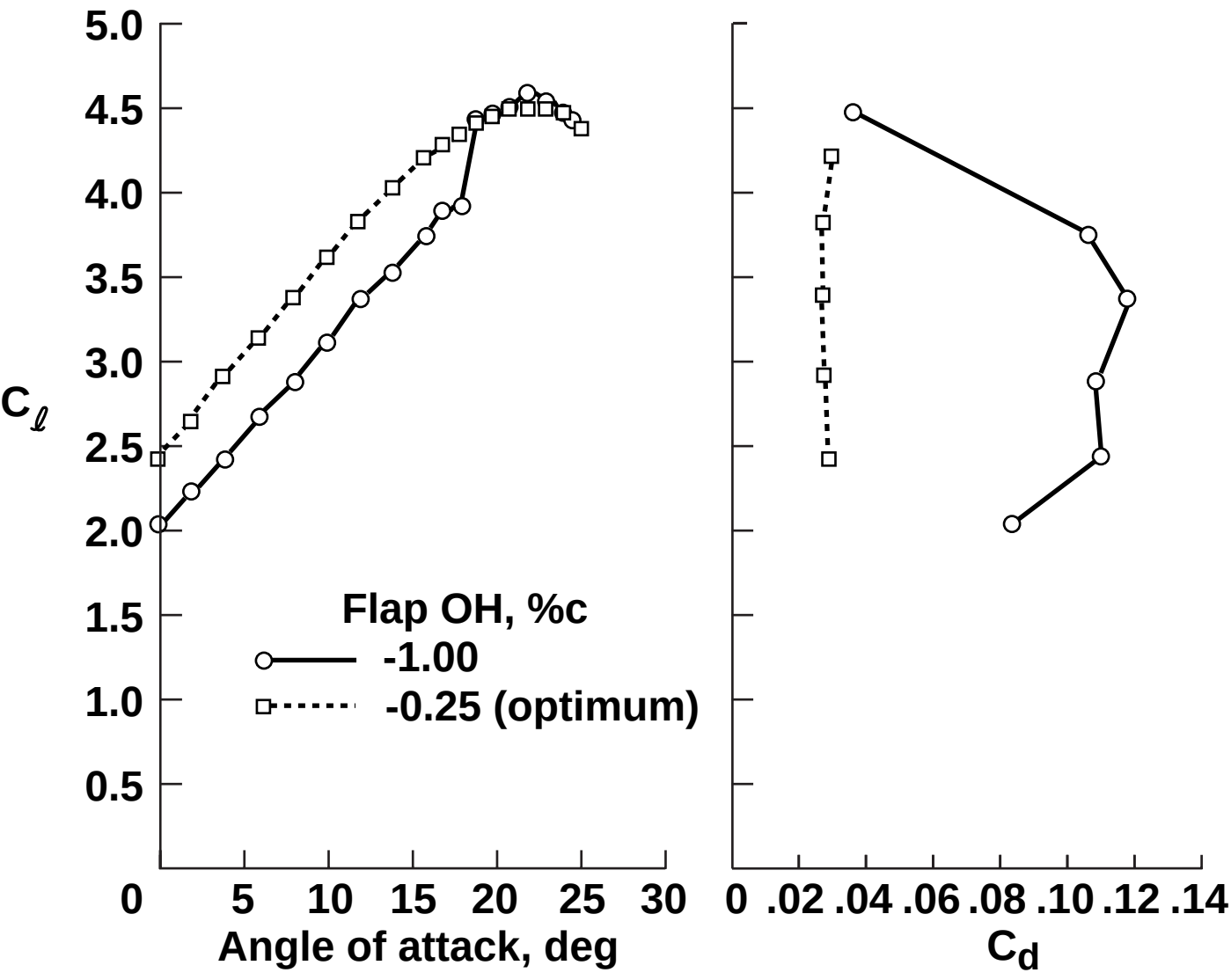

Fig. 17 Effect of flap overhang on lift and drag (Mach No. = 0.20, Reynolds No. = 16 million).

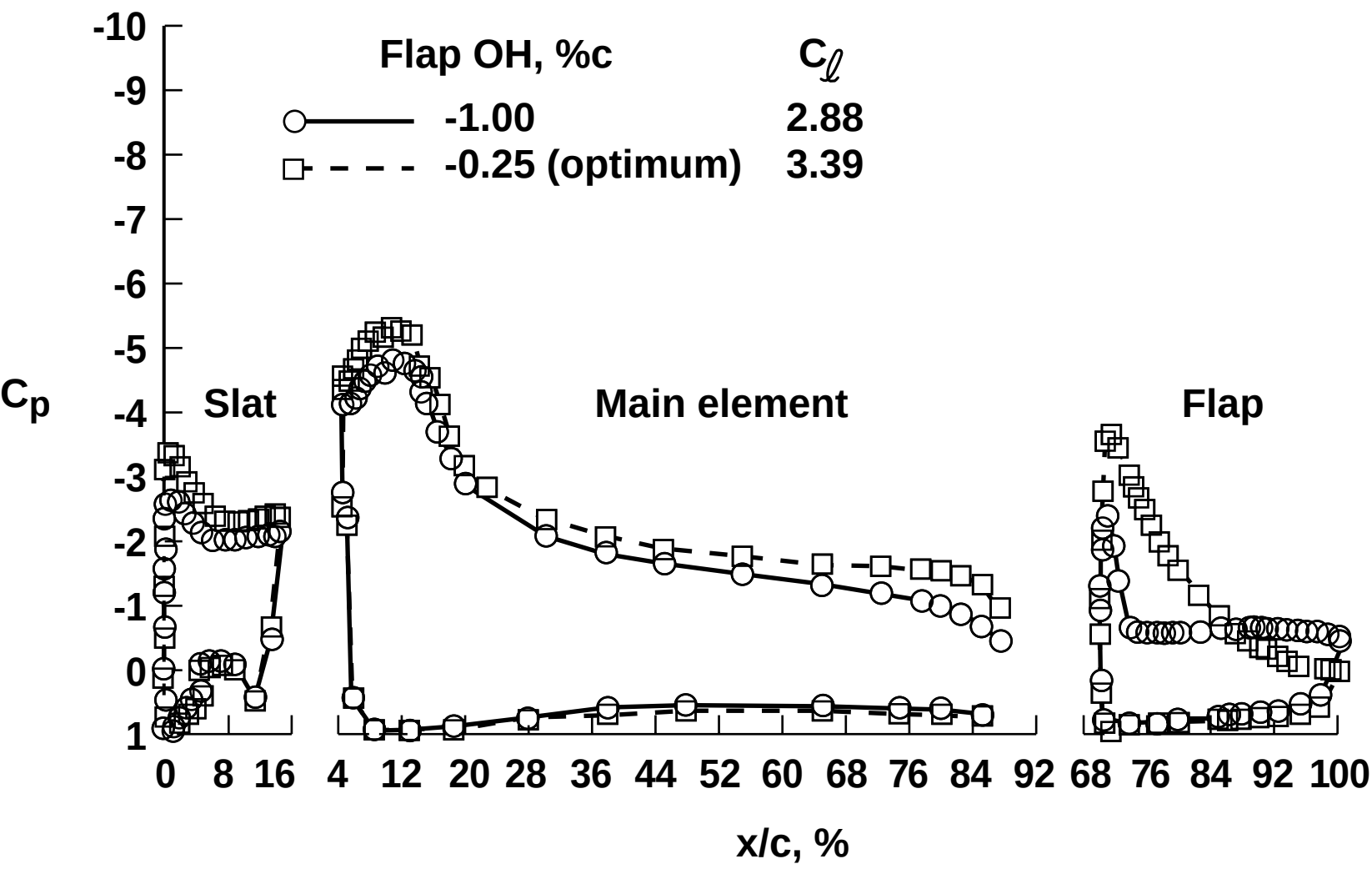

Fig. 18 Effect of flap overhang on surface pressures (Mach No. = 0.20, Reynolds No. = 16 million, angle of attack = 8 deg).

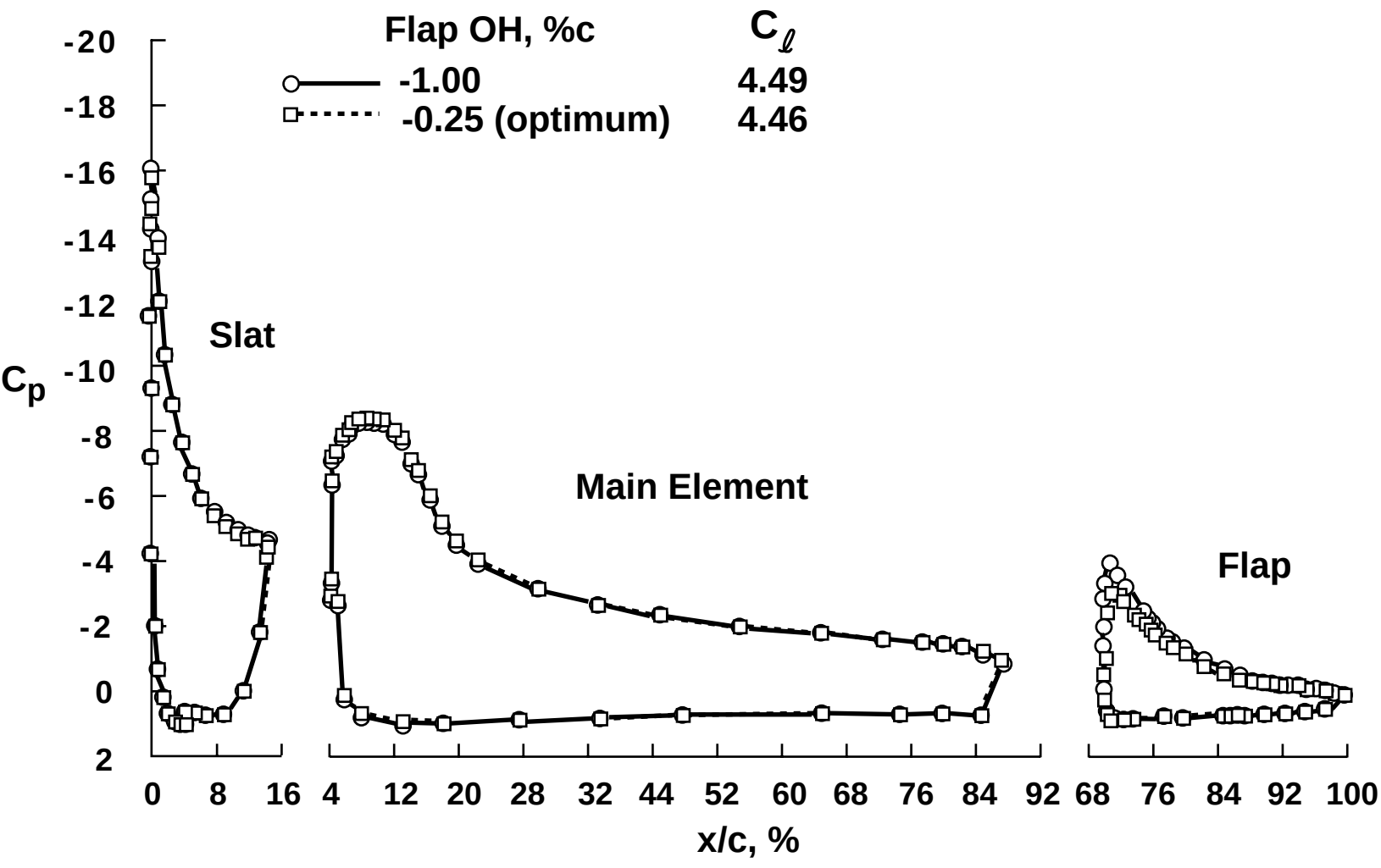

Fig. 19 Effect of flap overhang on surface pressures (Mach No. = 0.20, Reynolds No. = 16 million, angle of attack = 20 deg).

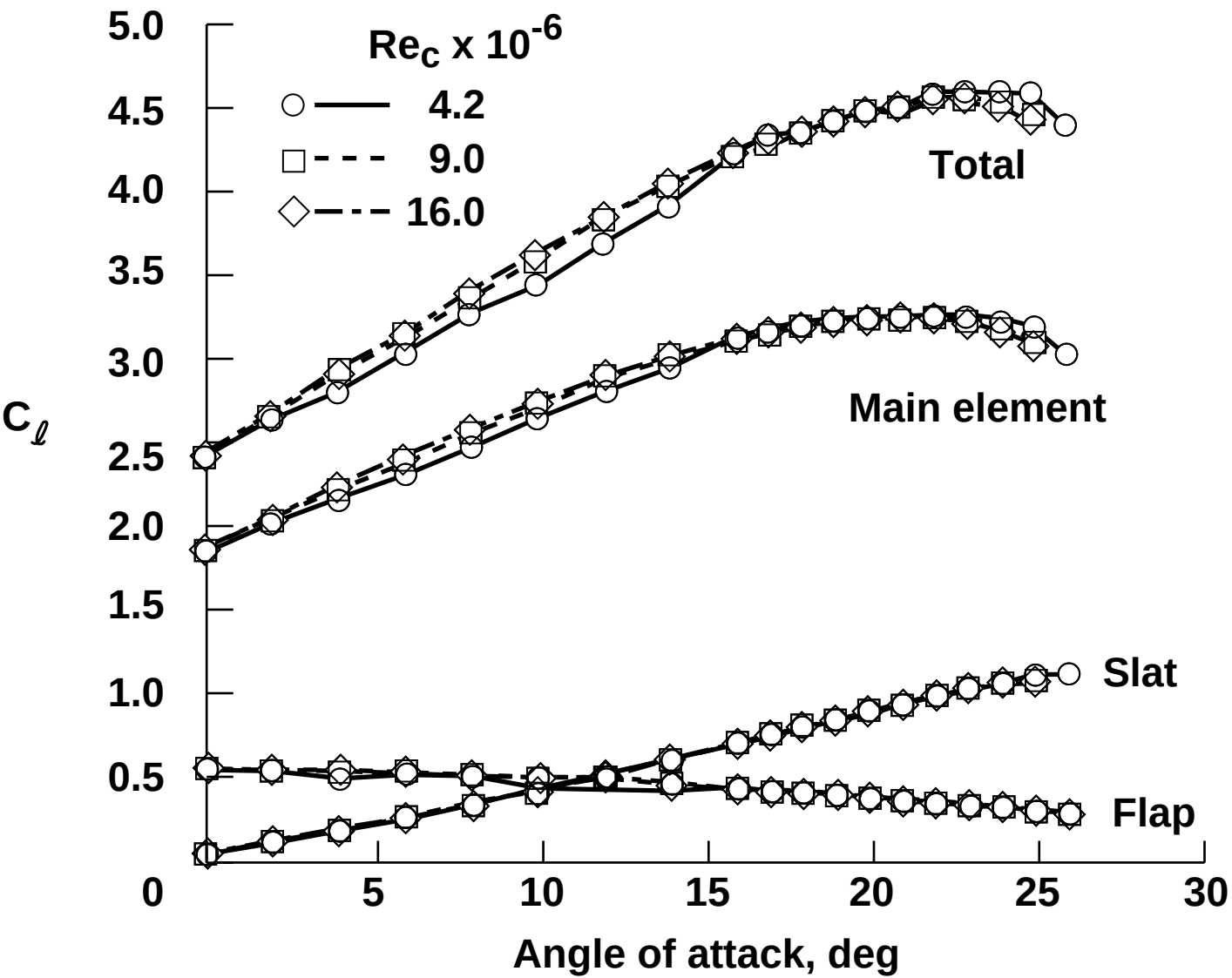

Fig. 20 Effect of Reynolds number on lift curves of optimum configuration (Mach No. = 0.20).

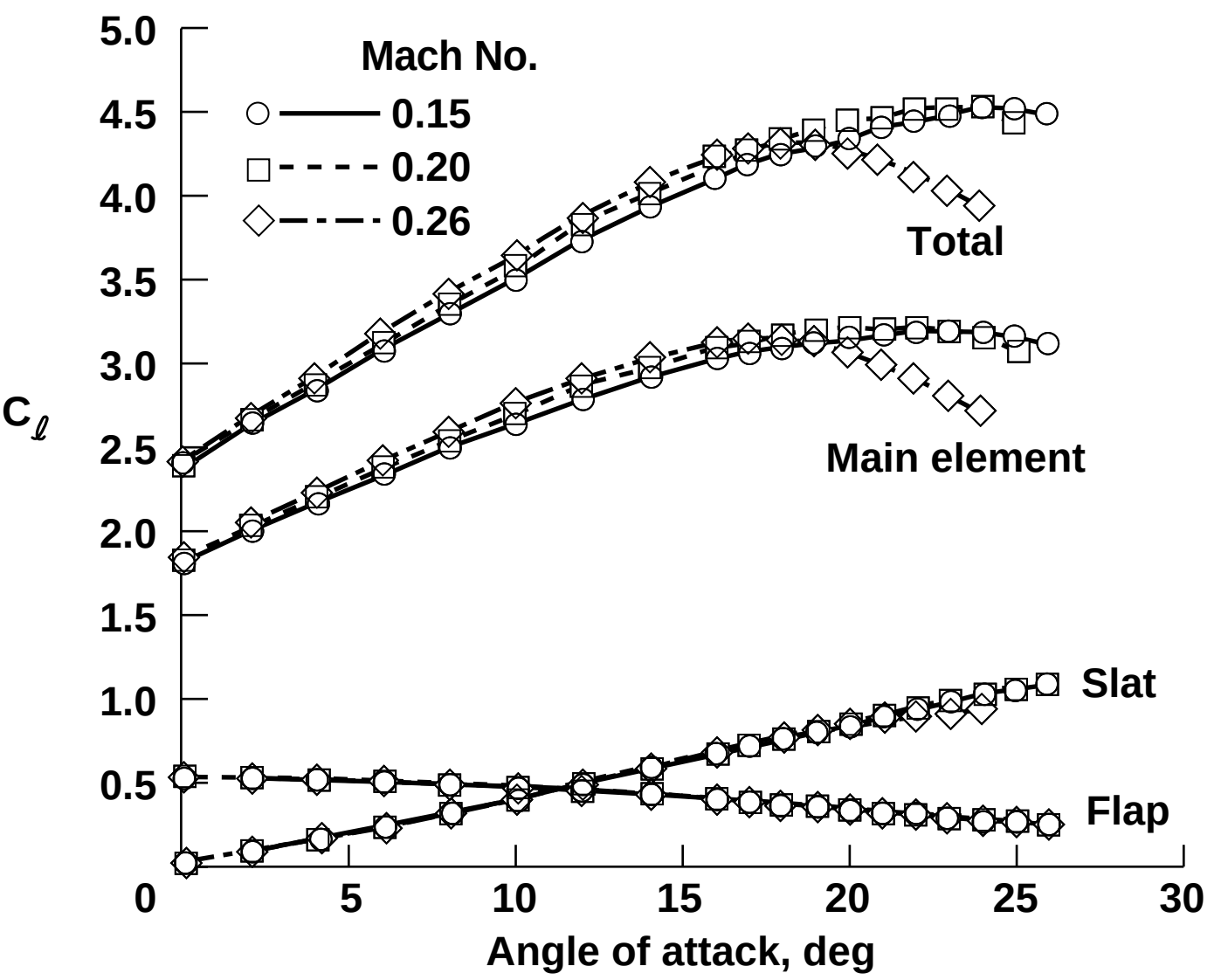

Fig. 21 Effect of Mach number on lift curves of optimum configuration (Reynolds No. = 9 million).

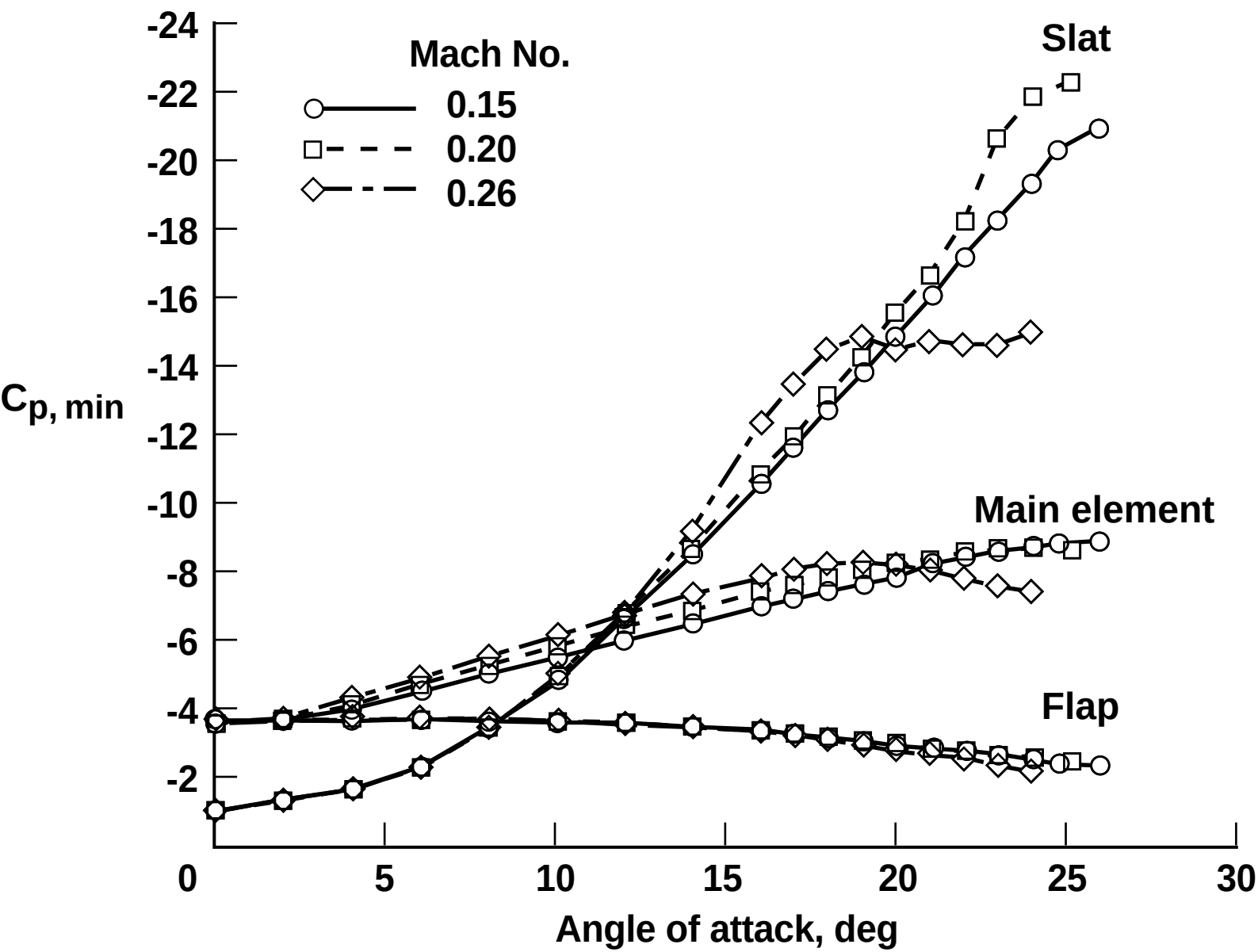

Fig. 22 Effect of Mach number on suction-peak pressures of optimum configuration (Reynolds No. = 9 million).